Full title: Mycobacterial infection-induced miR-206 inhibits protective neutrophil recruitment via the CXCL12/CXCR4 signalling axis

Short title: Infection-induced miR-206 expression is immunosuppressive

Kathryn Wright[1,2], Kumudika de Silva[2], Karren M. Plain[2], Auriol C. Purdie[2], Tamika A Blair[3], Iain G Duggin[3], Warwick J. Britton[1,4], Stefan H. Oehlers[1,5]*

[1]Tuberculosis Research Program at the Centenary Institute, The University of Sydney, Camperdown NSW Australia

[2]The University of Sydney, Faculty of Science, Sydney School of Veterinary Science, Sydney NSW, Australia

[3]ithree Institute, University of Technology Sydney, Ultimo, NSW, Australia

[4]Department of Clinical Immunology, Royal Prince Alfred Hospital, Camperdown, NSW, Australia

[5]The University of Sydney, Faculty of Medicine and Health & Marie Bashir Institute, Camperdown NSW Australia

* Corresponding author: Stefan Oehlers, stefan.oehlers@sydney.edu.au, Tuberculosis Research Program at the Centenary Institute, The University of Sydney, Camperdown NSW 2050 Australia

Abstract

Pathogenic mycobacteria actively dysregulate protective host immune signalling pathways during infection to drive the formation of permissive granuloma microenvironments. Dynamic regulation of host microRNA (miRNA) expression is a conserved feature of mycobacterial infections across host-pathogen pairings. Here we examine the role of miR-206 in the zebrafish model of *Mycobacterium marinum* infection, which allows investigation of the early stages of granuloma formation. We find miR-206 is upregulated following infection by pathogenic *M. marinum* and that antagomir-mediated knockdown of miR-206 is protective against infection. We observed striking upregulation of *cxcl12a* and *cxcr4b* in infected miR-206 knockdown

zebrafish embryos and live imaging revealed enhanced recruitment of neutrophils to sites of infection. We used Crispr/Cas9-mediated knockdown of *cxcl12a* and *cxcr4b* expression and AMD3100 inhibition of Cxcr4 to show that the enhanced neutrophil response and reduced bacterial burden caused by miR-206 knockdown was dependent on the Cxcl12/Cxcr4 signalling axis. Together, our data illustrate a pathway through which pathogenic mycobacteria induce host miR-206 expression to suppress Cxcl12/Cxcr4 signalling and prevent protective neutrophil recruitment to granulomas.

Author summary

Mycobacterial infections cause significant disease burden to humans and animals, the most widely known example being tuberculosis which has killed more humans than any other infectious disease throughout history. Infectious mycobacteria are highly evolved to hijack host processes, including the very immune cells tasked with destroying them. microRNAs are host molecules that control wide-ranging programs of host gene expression and are important in the immune response to infections. Here we use the zebrafish model of mycobacterial infection to determine the role of the infection-induced microRNA miR-206 in the host response to infection. We found pathogenic mycobacteria trigger the host to produce more miR-206 in order to suppress the otherwise protective recruitment of neutrophils to sites of infection via the host Cxcl12/Cxcr4 signalling pathway. Our study provides new insight into the role of mycobacterial infection-induced miR-206 function in the context of a whole host.

Introduction

Pathogenic mycobacteria, including the causative agents of tuberculosis and leprosy, are capable of appropriating host signalling and immune pathways to increase their survival and establish chronic infection in cell-rich granulomas, which support mycobacterial growth and latent survival (1, 2).

microRNA (miRNA) are short, non-coding RNA of approximately 22 nucleotides that can post-transcriptionally regulate gene expression and transcript abundance through “gene silencing”. miRNA bind to the untranslated region (UTR) of mRNA to regulate the stability of target genes through degradation or suppression, reducing protein translation (3). Expression of miRNA is dynamically regulated in mycobacterial infection, suggesting a key role in the

host response to infection by the modulation of downstream genes and protein expression (4-6).

miR-206 is a member of the muscle-associated myomiR family and is characteristically associated with myoblast differentiation and muscle development (7-10). However, miR-206 has been recently found to be differentially regulated in mycobacterial infection of THP-1 leukocytic cells (11). Infection of THP-1 cells with *Mycobacterium tuberculosis* revealed a role for miR-206 in the regulation of proinflammatory cytokine responses through reducing TIMP3 expression (11). miR-206 has also been implicated in viral pathogenesis, reducing replication of influenza virus, and in neuroinflammation (12, 13). While miR-206 clearly has a diverse range of biological functions, the *in vivo* role of miR-206 during mycobacterial infection remains undetermined.

Here we use the zebrafish-*Mycobacterium marinum* model to investigate the *in vivo* function of dre-miR-206-3p (miR-206) in mycobacterial infection, and the impact on host gene expression and neutrophil recruitment. Zebrafish are an established model for the investigation of host-mycobacteria interactions, and to evaluate host gene function, including the role of chemokine signalling (14-16). Regulation of neutrophil based inflammation and motility by miRNA has also been investigated using a zebrafish model (17-21), highlighting the applicability of the zebrafish model to study conserved miRNA functions within host-pathogen interactions.

Results

Zebrafish miR-206 expression is responsive to *M. marinum* infection

To determine if miR-206 is responsive to *M. marinum* infection in zebrafish, embryos were infected with *M. marinum* via caudal vein injection and miR-206 expression was measured by quantitative (q)PCR at 1, 3, and 5 days post infection (dpi). Infection with *M. marinum* increased miR-206 expression at 1 and 3 dpi, but decreased miR-206 expression at 5 dpi compared to uninfected controls (Fig 1A).

AntagomiR abrogates infection-induced miR-206 expression

To determine the efficacy of antagomiR-mediated miRNA knockdown during *M. marinum* infection, embryos were injected with miR-206 antagomiR at the single-cell stage and infected at 1.5 days post fertilisation (dpf). miR-206 expression levels were analysed at both 1- and 3-days post infection (dpi) and were increased in *M. marinum* infected embryos compared to control uninfected ($p=0.027$ and $p=0.039$ respectively). AntagomiR knockdown effectively reduced the miR-206 level relative to infected embryos at both timepoints, demonstrating effective knockdown of infection-induced miR-206 expression by antagomiRs (Fig 1B).

miR-206 knockdown reduces *M. marinum* burden

As miR-206 was modulated during infection, its effect on disease was assessed through assessing the bacterial burden following antagomiR knockdown. There was no difference in bacterial burdens between miR-206 knockdown and control embryos at 1 dpi, however by 3 dpi, knockdown embryos had a significantly lower burden than control embryos. (Fig 1C).

Infection-induced miR-206 upregulation is driven by mycobacterial virulence factors

To investigate whether the decreased bacterial burden in miR-206 knockdown embryos was a general response to foreign pathogens or a more directed response, embryos were infected with either ΔESX1 *M. marinum* or uropathogenic *Escherichia coli* (UPEC). ΔESX1 *M. marinum* lack the key type VII secretion system and are far less virulent as they are unable to lyse host cell membranes to escape the phagosome (22). In comparison to mycobacteria, UPEC cause an acute sepsis infection and are an example an extracellular bacterium.

Expression of miR-206 was analysed by qPCR in embryos infected with WT *M. marinum*, ΔESX1 *M. marinum*, or UPEC at 1 dpi (Fig 1D). Infection with ΔESX1 *M. marinum* increased miR-206 expression, however this response was less than the level induced by infection with virulent WT *M. marinum*. Conversely, miR-206 was decreased in embryos infected with UPEC.

ΔESX1 *M. marinum* infection burdens were unaffected by miR-206 knockdown at either 1 or 3 dpi (Fig 1E). Similarly, there was also no difference in UPEC burden levels in miR-206 knockdown embryos at either 6 hours post infection (hpi) or 1 dpi despite an increase

in infection between timepoints (Fig 1F). These results indicate that the impact on bacterial burden in miR-206 knockdown embryos is driven by *M. marinum* virulence factors.

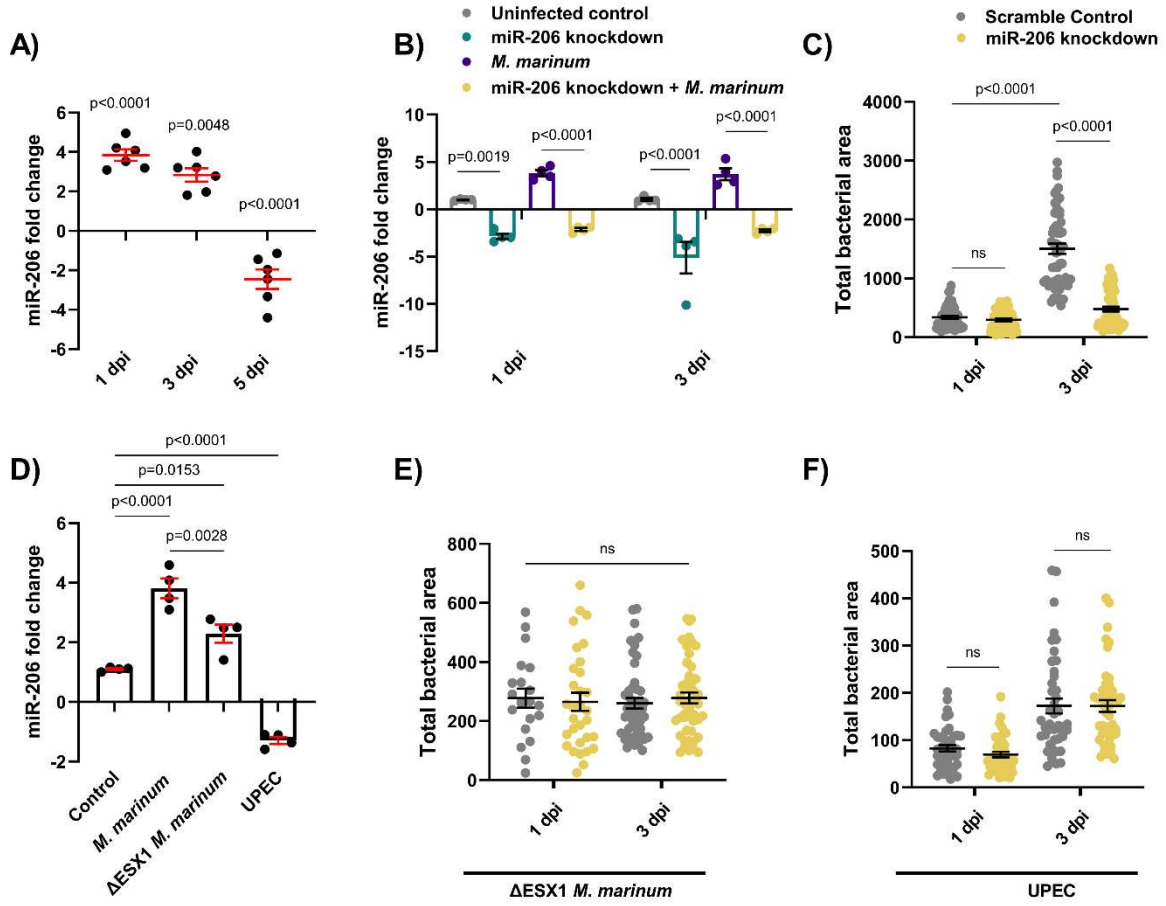

Fig 1. Infection-induced miR-206 expression alters bacterial burden. (A) Expression of miR-206 analysed by qPCR at 1, 3, and 5 dpi. (B) Expression of miR-206 in uninfected and infected antagomir-injected embryos (miR-206 knockdown). (C) *M. marinum* burden in miR-206 knockdown embryos at 1 and 3 dpi. (D) Expression of miR-206 at 1 dpi following infection with either wild-type (WT) *M. marinum*, ΔESX1 *M. marinum*, or UPEC. (E) ΔESX1 *M. marinum* burden in miR-206 knockdown embryos at 1 and 3 dpi. (F) UPEC burden in antagomir-injected embryos at 6 hpi and 1 dpi. Each data point represents a single measurement, with the mean and SEM shown. For qPCR analysis, each data point represents 10 embryos, and contains 2 biological replicates. Bacterial burden analysis data points (WT *M. marinum*, ΔESX1 *M. marinum,* and UPEC) represent individual embryos (n=40-50 embryos per group) and are representative of 2 biological replicates.

miR-206 target mRNA gene expression patterns are conserved during *M. marinum* infection of zebrafish

To further investigate the functional relevance of miR-206 in mycobacterial infection, a list of potential mRNA target genes was compiled through published experimentally observed targets and bioinformatic target prediction algorithms (23-26).

Expression of selected potential target genes of miR-206 was analysed by qPCR at 2 dpf, with increased expression in knockdown samples expected to indicate targeting by miR-206 (Fig 2A). From the expression profiling data, *cxcl12a* and *cxcr4b* were considered to be likely targets of miR-206. Expression of these genes was increased by *M. marinum* infection and in both knockdown treatments, suggesting they may be active during infection and contributing to the decreased bacterial burden observed in miR-206 knockdown embryos. These genes were also of particular interest as the Cxcl12/Cxcr4 pathway has been previously implicated in zebrafish immunity (14, 15). Expression of *cxcr4a, cxcr4b, cxcl12a* was analysed at 3 dpi, showing that knockdown of miR-206 significantly increased the transcript abundance of *cxcr4b* and *cxcl12a* in infected embryos compared to *M. marinum* infection alone and uninfected controls (Fig 2B-D).

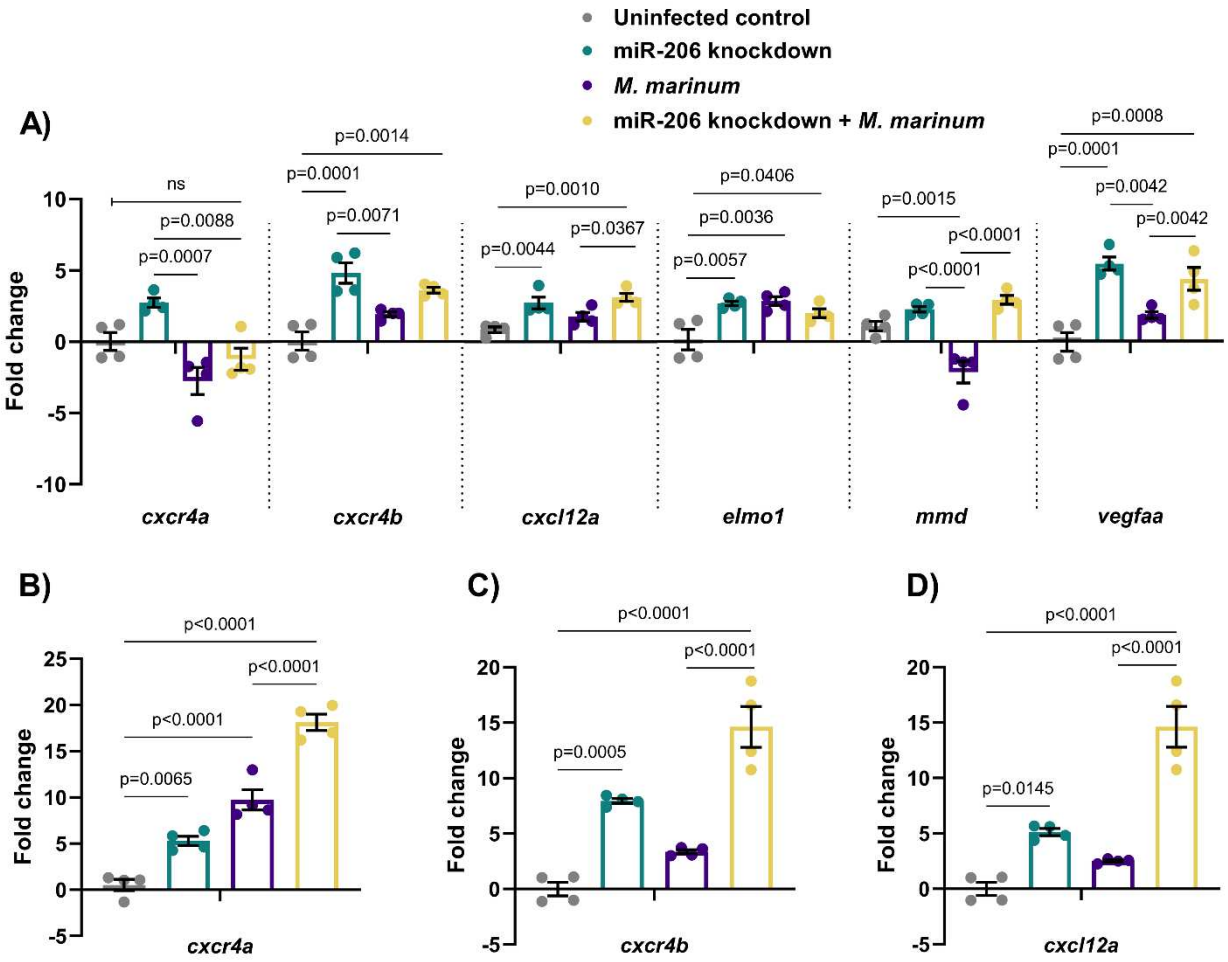

Fig 2. Expression profiles of potential mRNA targets of miR-206. (A) Expression of candidate target genes measured by qPCR at 1 dpi in miR-206 knockdown embryos. (B-D) Expression of zebrafish CXCL12/CXCR4 pathway ortholog genes at 3 dpi. Each data point represents a single measurement of 10 pooled embryos and 2 biological replicates, with the mean and SEM shown.

Knockdown of miR-206 increases neutrophil response to *M. marinum* infection

As miR-206 knockdown increased the expression of *cxcl12a* and *cxcr4* genes, which are involved in neutrophil migration and retention of cells at sites of infection and inflammation (19, 27-29), the neutrophil response to *M. marinum* infection in miR-206 knockdown treated embryos was assessed by live imaging of transgenic *Tg(lyzC:GFP)*^{nz117} or *Tg(lyzC:DsRed2)*^{nz50} embryos, where neutrophils are fluorescently labelled.

First, static imaging was performed at 1 and 3 dpi to measure total neutrophil numbers in infected embryos. At each timepoint, miR-206 knockdown embryos had a significantly higher total number of neutrophils compared to control (Fig 3A-B). We noted strong overlap of neutrophils with *M. marinum* but the location of granulomas around the caudal haematopoietic tissue confounded quantification of granuloma-associated neutrophils.

To determine if miR-206 knockdown increased the number of infection-associated neutrophils, embryos were injected with *M. marinum* into the trunk (away from the caudal haematopoietic tissue) and subjected to time-lapse imaging (30). Knockdown embryos had significantly more neutrophils at the site of infection for the first 2.5 hours of infection compared to control infected embryos (Fig 3C). While neutrophil migration in control infected embryos began to wane at approximately 12 hpi (S1 video), the response in the knockdown embryos was sustained and higher numbers of neutrophils were maintained at the site of infection (S2 video).

To examine if the increased mobilisation of neutrophils in the *M. marinum*-infected miR-206 knockdown embryos was dependent on mycobacterial infection cues or an intrinsic feature of neutrophils in miR-206-depleted animals, we assessed neutrophil migration to a sterile tail fin wound as an example of a non-infectious inflammatory stimulus (Fig 3D). The number of neutrophils at the wound site did not significantly differ between scramble control (S3 video) and miR-206 knockdown embryos (S4 video), indicating the increased neutrophil response observed in trunk infections is *M. marinum* infection-dependent.

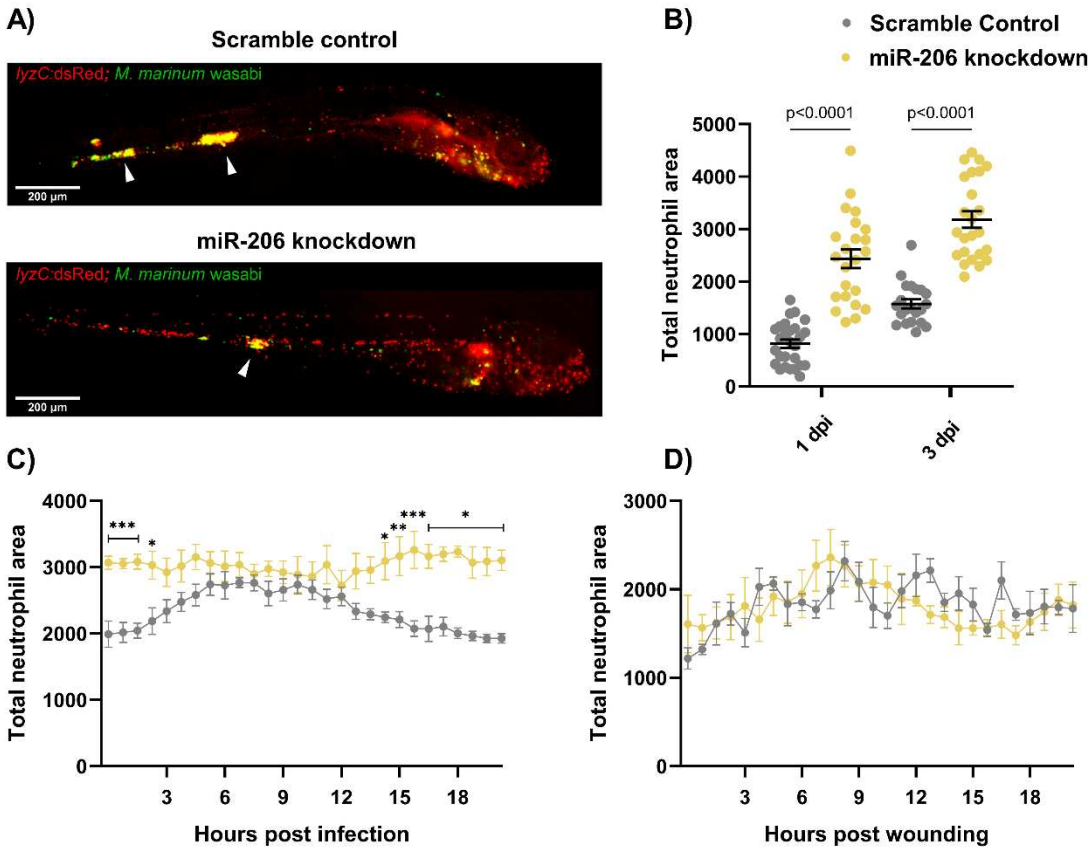

Fig 3. Infection-induced miR-206 expression alters the host neutrophil response. (A) Representative images of infection phenotype at 3 dpi in control and miR-206 knockdown embryos. White arrows indicate bacterial foci. Neutrophils are red (*lyzC:dsred*) and *M. marinum* is green (wasabi); co-localisation is indicated by yellow fluorescence. (B) Measurement of whole-body neutrophil fluorescent area at 1 and 3 dpi in miR-206 knockdown embryos. (C) Measurement of neutrophil levels following trunk infection with *M. marinum* in miR-206 knockdown embryos. (D) Measurement of neutrophil recruitment to a sterile tail fin wound in miR-206 knockdown embryos. Each data point represents a single measurement, with the mean and SEM shown. For time-lapse imaging, each data point represents the mean of 6 foci of infection from 6 separate embryos. Bacterial burden analysis was performed on 15-20 embryos per treatment. Graphs are representative of 2 biological replicates. * $P < 0.05$, ** $p < 0.01$, *** $p < 0.001$

The Cxcr4/Cxcl12 signalling axis is downstream of miR-206 in *M. marinum* infection

To confirm the hypothesised link between the observed increased transcription of *cxcr4b* and *cxcl12a* and reduced bacterial burden through an increased neutrophil response early in

200 infection, both genes were targeted for knockdown by Crispr-Cas9. As both *cxcr4b* and *cxcl12*
201 are involved in neutrophil migration and haematopoiesis, a reduction in their expression was
202 expected to result in a reduced neutrophil response to infection and therefore an increased
203 bacterial burden, reducing the protective effect of miR-206 knockdown.

204 Static imaging at 3 dpi revealed that double knockdown of *cxcr4b* and miR-206 ablated
205 the increased neutrophil number associated with miR-206 knockdown (Fig 4A). Furthermore,
206 addition of *cxcr4b* knockdown to miR-206 knockdown dampened the miR-206 knockdown-
207 induced increase in neutrophil recruitment to a trunk infection and increased bacterial burden
208 back to control levels (Fig 4B-C). The effect observed in the double knockdown is consistent
209 with a reduction in Cxcr4 and therefore the neutrophil response in infection via haematopoiesis
210 and chemoattraction. This suggests the miR-206 associated increase in *cxcr4b* is contributing
211 to the enhanced neutrophil migration and reduced bacterial burden.

212 To further confirm involvement of Cxcr4 downstream of miR-206, the CXCR4
213 antagonist AMD3100 was used to pharmacologically block Cxcr4 signalling. AMD3100
214 treatment reduced the total neutrophil numbers in all treatment groups, and as expected, whole-
215 body neutrophil counts were reduced in miR-206 knockdown embryos that were also treated
216 with AMD3100 compared to miR-206 knockdown alone (Fig 4D). AMD3100 treatment
217 decreased neutrophil recruitment to the site of infection compared to both control infected and
218 miR-206 knockdown infected embryos (Fig 4E). Bacterial burden was increased in AMD3100
219 treated embryos and AMD3100 treatment of miR-206 knockdown embryos restored bacterial
220 burden to control levels (Fig 4F).

221

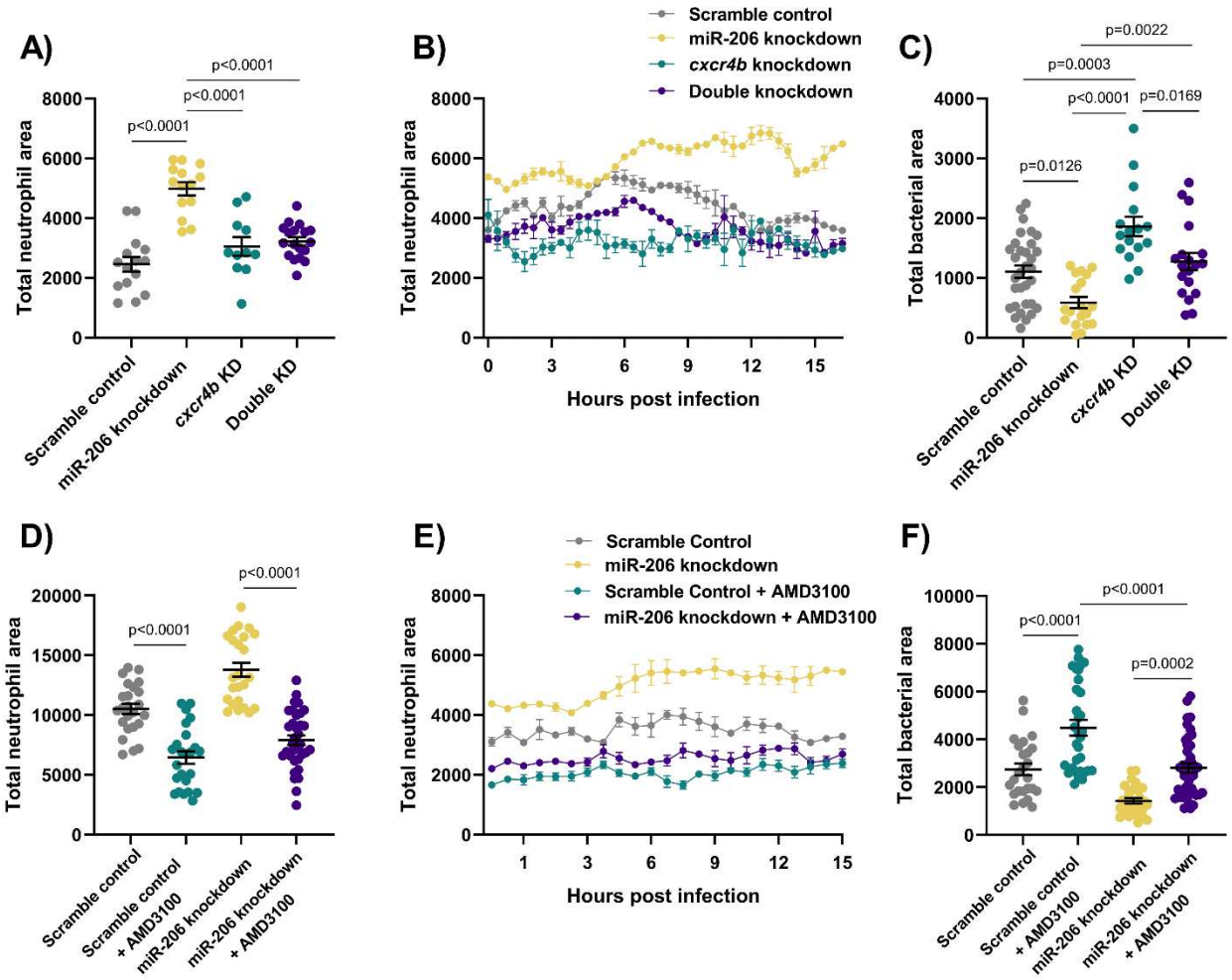

Fig 4. Cxcr4 reduction places the Cxcl12/Cxcr4 signalling axis downstream of miR-206. (A) Whole body neutrophil counts at 3 dpi of *cxcr4b* and double (*cxcr4b* and miR-206) knockdown embryos. (B) Measurement of neutrophil levels following trunk infection with *M. marinum* in double knockdown embryos. (C) Bacterial burden at 3 dpi in *M. marinum*-infected double knockdown embryos. (D) Whole body neutrophil counts at 3 dpi in miR-206 knockdown embryos treatment with AMD3100. (E) Measurement of neutrophil recruitment to *M. marinum* following trunk injection in miR-206 knockdown embryos treatment with AMD3100. (F) Bacterial burden at 3 dpi in miR-206 knockdown embryos treatment with AMD3100. Each data point represents a single measurement, with the mean and SEM shown. For time-lapse imaging, each data point represents the mean of 6 foci of infection from 6 separate embryos. Bacterial burden analysis was performed on 15-25 embryos per treatment. Graphs are representative of 2 biological replicates, except for AMD3100 data, which is a single biological replicate.

Consistent with the results of *cxcr4b* knockdown, addition of *cxcl12a* knockdown to miR-206 knockdown decreased the total number of neutrophils and number of neutrophils recruited to sites of infection compared to miR-206 knockdown alone (Fig 5A-B), and increased the bacterial burden compared to miR-206 knockdown alone (Fig 5C).

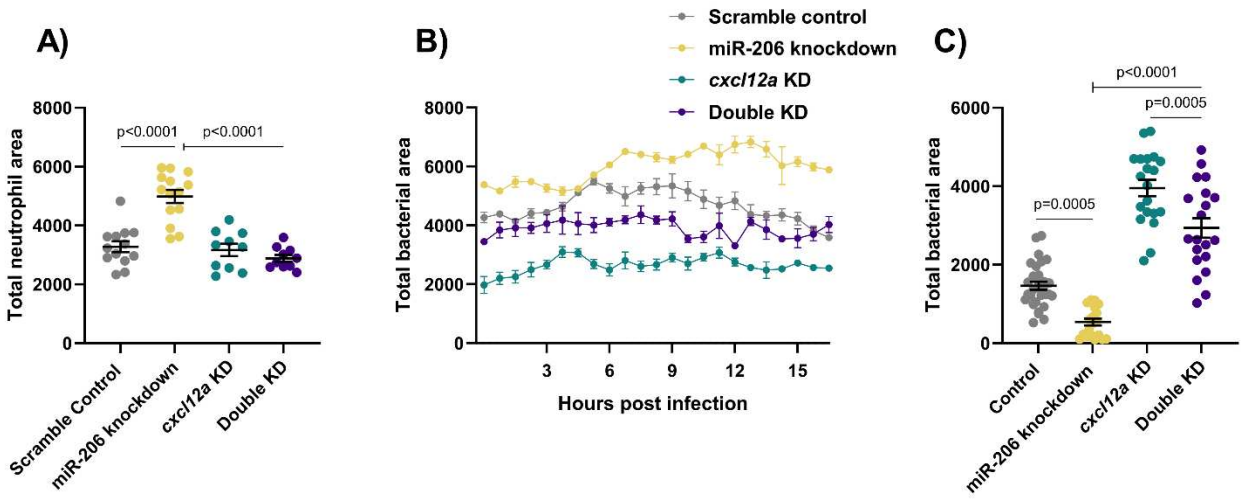

Fig 5. Cxcl12a knockdown places the Cxcl12/Cxcr4 signalling axis downstream of miR-206. (A) Whole body neutrophil counts at 3 dpi of *cxcl12a* and double (*cxcl12a* and miR-206) knockdown embryos. (B) Measurement of neutrophil recruitment to *M. marinum* following trunk injection in double knockdown embryos. (C) Bacterial burden at 3 dpi in *M. marinum*-infected double knockdown embryos. Each data point represents a single measurement, with the mean and SEM shown. For time-lapse imaging, each data point represents the mean of 4 foci of infection from 4 separate embryos. Bacterial burden analysis was performed on 20-30 embryos per treatment. Graphs are representative of 2 biological replicates.

Discussion

In this study we have demonstrated an *in vivo* link between infection-induced miR-206 expression and the Cxcl12/Cxcr4 signalling axis in the control of mycobacterial infection. Knockdown of miR-206 resulted in a decreased bacterial burden and improved infection outcome. We attribute the reduced bacterial burden to an increased early neutrophil response from increased *cxcr4b* and *cxcl12a* transcript abundance in miR-206 knockdown animals. We show that host miR-206 is increased by pathogenic *M. marinum* to impede the host Cxcl12/Cxcr4 signalling axis, thereby reducing protective early neutrophil recruitment to the site of infection and aiding the creation of a permissive niche for mycobacterial infection.

As this early protective neutrophil response was specific to virulent intracellular mycobacteria, the observed increase in miR-206 was deemed to be ESX1-dependent. We hypothesise that this may be a mycobacteria-driven response to avoid neutrophil phagocytosis and potentially oxidative killing (31). Neutrophils are one of the first immune cells to respond to mycobacterial infection and are capable of both phagocytosing and trapping mycobacteria in neutrophil extracellular traps (32). Therefore, it is not surprising that mycobacteria have evolved a strategy to actively subvert host neutrophil recruitment by reducing Cxcl12/Cxcr4 signalling, limiting the downstream exposure of mycobacteria to phagocytosis and oxidative killing.

Involvement of Cxcr4 and its ligand Cxcl12 in inflammation is well documented (33-35), however, previous studies have largely focused on their role in viral responses. Cxcr4 expression is reduced in the lymphocytes of leprosy patients, but increased in *M. tuberculosis*-infected macrophages (36, 37). Recent work has highlighted Cxcr4 as a mediator of host infection-associated angiogenesis (38), while this study further links the Cxcl12/Cxcr4 signalling axis to virulence-dependent neutrophil recruitment during mycobacterial infections. Cxcr4 has also been shown to participate in pathogen immune evasion via interaction with TLR2, suggesting it may play an active role in other aspects of mycobacterial pathogenesis (39).

Our data provide precedence for cross-species conservation of host miRNA responses to mycobacterial infection. Although current understanding of the role of miR-206 in bacterial infections has been limited to date, previous investigation using *M. tuberculosis* infection of THP-1 cells revealed a similar infection-induced upregulation of miR-206 *in vitro* (11). Our *in vivo* model of mycobacterial infection has allowed the interrogation of neutrophil responses as a downstream cellular response controlled by miR-206.

While we have demonstrated the effect of miR-206 expression on *cxcl12a* and *cxcr4b*, other genes targeted by miR-206 may also contribute to host control of mycobacterial infection. One validated target of miR-206, Vegf, plays a significant role in the later development of granulomas during mycobacterial infection, consistent with the late downregulation of miR-206 that we observed (24, 26, 40). Infection-induced Vegf signalling results in an aberrant angiogenesis programme which favours mycobacterial growth and spread (30, 41-43). This effect may be synergistic with Cxcl12/Cxcr4 signalling, which supports granuloma-associated angiogenesis through a Vegf-independent mechanism (38).

In addition, suppression of *elmo1* by miR-206 may further contribute to the immune avoidance associated with the infection-induced increase in miR-206. Recent investigations have revealed a role for Elmo1 in neutrophil migration and engulfment of apoptotic cells (44) and this has been linked to enhanced intracellular mycobacterial growth (45). Increased transcription of Elmo1 following miR-206 knockdown is likely to increase neutrophil mobility during infection in cooperation with increased Cxcl12/Cxcr4 signalling.

miR-206 may also act on *timp3* to inhibit the activity of Mmp9 during mycobacterial infection (11), preventing macrophage recruitment and granuloma formation in our miR-206 knockdown model (46). However, dissecting the miR-206-Mmp9 interaction may require a different experimental platform to determine if reduced *mmp9* expression is a result of transcriptional feedback from its inhibitor Timp3 or caused by the reduced bacterial burden. This may prove to be an additional pathway modulated by miR-206 during infection, acting to alter disease progression and highlights the complex interaction of miRNA and their multiple targets.

The final potential target gene we profiled, *mmd,* may also be of significance through the positive regulation of macrophage activation and downstream cytokine signalling cascades (47).

In summary, we have identified potential target genes of miR-206 which may be biologically active during mycobacterial infection. We have demonstrated a link between infection-associated upregulation of miR-206 and suppression of neutrophil recruitment to the site of pathogenic mycobacterial infection involving the Cxcl12/Cxcr4 signalling pathway. This host response to infection by pathogenic mycobacteria appears to be conserved across host-pathogen pairings and could inform the development of biomarker or therapeutic strategies.

Methods

1. Zebrafish husbandry

Adult zebrafish were housed at the Centenary Institute and experiments were approved by Sydney Local Health District AWC Approval 17-036. The embryos were obtained by natural spawning and were raised in E3 media and maintained at 28-32°C.

2. Zebrafish lines

Zebrafish were AB strain. Transgenic lines used were: *Tg(lyzC:GFP)*^{nz117} and *Tg(lyzC:DsRed2)*^{nz50} were used for neutrophil imaging experiments (48).

3. Embryo microinjection with antagomiR

Embryos were obtained by natural spawning and were injected with either miR-206 antagomiR (-CCACACACUUCCUUACAUUCCA-) or a scramble control (-CAGUACUUUUGUGUAGUACAA-) (GenePharma, China) at 200 pg/embryo at the single cell stage and maintained at 32°C.

4. miRNA target prediction

Prediction of target mRNA was performed using TargetScan. dre-miR-206-3p was entered into TargetScanFish 6.2 (http://www.targetscan.org/fish_62/), hsa-miR-206 entered into TargetScan 7.2 (http://www.targetscan.org/vert_72/), and mmu-miR-206 entered into TargetScanMouse 7.2 (http://www.targetscan.org/mmu_72/).

5. *M. marinum* culture

M. marinum was cultured and quantified as previously described (49). *M. marinum* expressing Wasabi or tdTomato fluorescent protein was used for infections.

6. UPEC culture

Uropathogenic *Escherichia coli* (UPEC) carrying the mCherry PGI6 plasmid was cultured in LB supplemented with 50 µg/mL of spectinomycin overnight at 37°C with 200 RPM shaking. Bacteria was then further diluted 1:10 with LB + spectinomycin (50 µg/ml) and incubated for 3 hours at 37°C with 200 RPM shaking. 1 mL of culture was centrifuged (16,000 x *g* for 1 minute), and the pellet washed in PBS. Following another centrifugation, the bacterial pellet was resuspended in 300 µl of PBS + 10% glycerol and aliquoted for storage. Enumeration of

bacteria was performed by serial dilution on LB + spectinomycin agar plates and culturing at 37°C overnight. Bacterial concentration was determined by CFU counts.

7. UPEC plasmid construction

The plasmid pGI6 was constructed by replacing the open reading frame (ORF) of msfGFP in pGI5 (50) with an E. coli codon-optimised ORF for mCherry. The mCherry ORF was first amplified with the forward primer (GCG CCG CCA TGG GTG AGC AAG GGC GAG GAG GAT) and reverse primer (GGC CCG GGA TCC TTA CTT GTA CAG CTC GTC CAT GCC) from the template pIDJL117 (51). The PCR fragment was cloned at NcoI and BamHI in pGI5, thus replacing msfGFP, and the PCR-generated confirmed by sequencing.

8. Bacterial infections

Staged at approximately 1.5 dpf, embryos were dechorionated and anesthetised in tricaine (160 µg/ml). Working solutions of *M. marinum* or UPEC (diluted with 0.5% w/v phenol red dye) were injected into either the caudal vein or trunk to deliver approximately 200 CFU *M. marinum* or 250 CFU UPEC. Embryos were recovered in E3 media + PTU (0.036 g/L) and housed at 28°C.

9. Crispr-Cas9 mediated knockdown

Embryos were injected at the 1-2 cell stage with 1 nL of Crispr mixture containing 1 µg/µl Guide (g) RNA (Table 1.), 500 µg/mL Cas9. For double knockdowns with Crispr-Cas9 and antagomiR, mixtures contained 1 µg/µl gRNA, 100 pg/nL antagomiR (miR-206), and 500 µg/mL Cas9. gRNA was synthesised as previously described (52). Embryos were transferred to E3 containing methylene blue and maintained at 32°C.

Table 1. Guide RNA sequences used for Crispr-Cas9 mediated knockdown experiments

Target	Primer
cxcr4b target 1	TAATACGACTCACTATAGGAGCTCTGACTCCGGTTCTGTTTTAGAGCTAGAAATAGC
cxcr4b target 2	TAATACGACTCACTATAGGACTGCAAGATAGCGGTCCGTTTTAGAGCTAGAAATAGC

cxcr4b target 3	TAATACGACTCACTATAGGGTACCCATGCTCGAATTGGTTTTAGAGCTAGAAATAGC
cxcr4b target 4	TAATACGACTCACTATAGGCTTACTGTGCCGGCATCCGTTTTAGAGCTAGAAATAGC
cxcl12a target 1	TAATACGACTCACTATAGGTCGTAGTAGTCGCTCTGAGTTTTAGAGCTAGAAATAGC
cxcl12a target 2	TAATACGACTCACTATAGGTCATGCACCGATTTCCAAGTTTTAGAGCTAGAAATAGC
cxcl12a target 3	TAATACGACTCACTATAGGATACTCACATGACTTGGAGTTTTAGAGCTAGAAATAGC
cxcl12a target 4	TAATACGACTCACTATAGGGCAGATACTCACATGACTGTTTTAGAGCTAGAAATAGC

10. Gene expression analysis

Groups of 10 embryos were lysed and homogenised using a 27-gauge needle in 500 µl Trizol (Invitrogen) and RNA extracted as per the manufacturer's instructions. cDNA was synthesised from 500 ng RNA using the miScript II RT kit (Qiagen) with HiFlex buffer. qPCR was carried out on an Mx3000p Real-time PCR system using Quantitect SYBR Green PCR Mastermix and primer concentration of 300 nM (Table 2.). For miRNA qPCRs, the miScript Universal Primer was used alongside miR specific miScript primer assays (miR-206 cat. no. MS00001869 and U6 cat. no. MS00033740; Qiagen).

Table 2. qPCR primer sequences

qPCR Primer	Sequence 5'-3'	Ensembl ID
cxcr4a forward	CAGTTTGGACCGGTACCTCG	ENSDARG00000057633
cxcr4a reverse	CCAGGTGACAAACGAGTCCT	
cxcr4b forward	TCGCAGACCTCCTGTTTGTC	ENSDARG00000041959
cxcr4b reverse	CCTTCCCGCAAGCAATTTCC	
cxcl12a forward	ATTCGCGAGCTCAAGTTCCT	ENSDARG00000037116
cxcl12a reverse	ATATCTGTGACGGTGGGCTG	
elmo1 forward	TGTTGACCATGCGTCTCAGT	ENSDARG00000098753
elmo1 reverse	CCACCTTCACGATGTCTGCC	
mmd forward	GGGGGTCTGGTCTACTGTCT	ENSDARG00000040387
mmd reverse	TTGTTAGTGGCTCAGGCGTC	
vegfaa forward	TCCCGACAGAGACACGAAAC	ENSDARG00000045971
vegfaa reverse	TTTACAGGTGAGGGGGTCCT	
b-actin forward	CCTTCCAGCAGATGTGGATT	ENSDARG00000037870
b-actin reverse	CACCTTCACCGTTCCAGTTT	

Cycling conditions for miRNA were: 95°C for 15 minutes; 40 cycles of 95°C for 20 seconds, 56°C for 30 seconds, 72°C for 30 seconds with fluorescence data acquisition occurring at the end of each cycle, followed by 1 cycle of 95°C for 1 minute, 65°C for 30 seconds, and 97°C for 30 seconds. For mRNA, the conditions were: 95°C for 15 minutes; 40 cycles of 94°C for 15 seconds, 55°C for 30 seconds, 70°C for 30 seconds with fluorescence data acquisition occurring at the end of each cycle, followed by 1 cycle of 95°C for 1 minute, 65°C for 30 seconds, and 97°C for 30 seconds.

U6 or β-actin was used as an endogenous control for normalisation and data analysed using the $2^{-\Delta\Delta}$ Ct method.

11. AMD3100 treatment

Embryos were treated with 20 μM AMD3100 (Sigma-Aldrich), a pharmacological CXCR4 antagonist, dissolved in water and refreshed daily.

12. Static imaging and burden analyses

Live imaging was performed on anaesthetised embryos on a depression microscope slide. Images were acquired using a Leica M205FA Fluorescent Stereo Microscope equipped with a Leica DFC365FX monochrome digital camera (Leica Microsystems, Germany). Images were analysed using ImageJ software to quantify the fluorescent pixel count (49).

13. Neutrophil tracking analyses

Time-lapse imaging was performed on a Deltavision Elite at 28°C (GE, USA). Following infection with *M. marinum* into the trunk, embryos were mounted in a 96-well black-walled microplate in 1% low-melting point agarose topped up with E3. Images were captured every 60-180 seconds for 16-24 hours. Analysis was performed using ImageJ software. Briefly, every 10-30 images were analysed for the quantity of neutrophils in a 1000 x 500 μm box around infection foci by quantifying the fluorescent pixel count (total neutrophil area) at each time point.

14. Statistics

Statistical analysis was performed in GraphPad Prism (v. 9.0.0). All data was analysed by T-test or ANOVA depending on the number of experimental groups, post-hoc analysis performed using Tukey's multiple comparisons test. For time-lapse data, group comparisons were computed using the Sidak test. Outliers were removed prior to statistical analysis using ROUT, with Q=1%.

Acknowledgements

Dr Angela Kurz of the BioImaging Facility and Sydney Cytometry at Centenary Institute for technical assistance with imaging, Dr Pradeep Manuneedhi Cholan for assistance with imaging, and Dr Elinor Hortle for assistance with image analysis.

Author contributions

KW, KDS, KMP, ACP, WJB, SHO conceived the experiments. KW and SHO designed the experiments. IGD and TAB created and provided essential reagents. KW performed the experiments. KW and SHO analysed the data. KW and SHO wrote the paper that was read and approved by all authors.

References

1. Hortle E, Oehlers SH. Host-directed therapies targeting the tuberculosis granuloma stroma. Pathogens and Disease. 2020;78(2).
2. Ramakrishnan L. Revisiting the role of the granuloma in tuberculosis. Nature Reviews Immunology. 2012;12(5):352-66.
3. Duchaine TF, Fabian MR. Mechanistic Insights into MicroRNA-Mediated Gene Silencing. Cold Spring Harbor Perspectives in Biology. 2018.
4. Behrouzi A, Alimohammadi M, Nafari AH, Yousefi MH, Riazi Rad F, Vaziri F, et al. The role of host miRNAs on Mycobacterium tuberculosis. ExRNA. 2019;1(1):40.
5. Han SA, Jhun BW, Kim S-Y, Moon SM, Yang B, Kwon OJ, et al. miRNA Expression Profiles and Potential as Biomarkers in Nontuberculous Mycobacterial Pulmonary Disease. Scientific Reports. 2020;10(1):3178.
6. Sabir N, Hussain T, Shah SZA, Peramo A, Zhao D, Zhou X. miRNAs in Tuberculosis: New Avenues for Diagnosis and Host-Directed Therapy. Frontiers in microbiology. 2018;9:602-.

7. Anderson C, Catoe H, Werner R. MIR-206 regulates connexin43 expression during skeletal muscle development. Nucleic acids research. 2006;34(20):5863-71.
8. Boettger T, Wüst S, Nolte H, Braun T. The miR-206/133b cluster is dispensable for development, survival and regeneration of skeletal muscle. Skeletal Muscle. 2014;4(1):23.
9. Kim HK, Lee YS, Sivaprasad U, Malhotra A, Dutta A. Muscle-specific microRNA miR-206 promotes muscle differentiation. The Journal of Cell Biology. 2006;174(5):677.
10. Ma G, Wang Y, Li Y, Cui L, Zhao Y, Zhao B, et al. MiR-206, a key modulator of skeletal muscle development and disease. Int J Biol Sci. 2015;11(3):345-52.
11. Fu X, Zeng L, Liu Z, Ke X, Lei L, Li G. MicroRNA-206 regulates the secretion of inflammatory cytokines and MMP9 expression by targeting TIMP3 in Mycobacterium tuberculosis–infected THP-1 human macrophages. Biochemical and Biophysical Research Communications. 2016;477(2):167-73.
12. Bamunuarachchi G, Yang X, Huang C, Liang Y, Guo Y, Liu L. MicroRNA-206 inhibits influenza A virus replication by targeting tankyrase 2. Cellular Microbiology. 2020;n/a(n/a):e13281.
13. Duan X, Zohaib A, Li Y, Zhu B, Ye J, Wan S, et al. miR-206 modulates lipopolysaccharide-mediated inflammatory cytokine production in human astrocytes. Cellular Signalling. 2015;27(1):61-8.
14. Torraca V, Cui C, Boland R, Bebelman J-P, van der Sar AM, Smit MJ, et al. The CXCR3-CXCL11 signaling axis mediates macrophage recruitment and dissemination of mycobacterial infection. Disease Models & Mechanisms. 2015;8(3):253-69.
15. Torraca V, Otto NA, Tavakoli-Tameh A, Meijer AH. The inflammatory chemokine Cxcl18b exerts neutrophil-specific chemotaxis via the promiscuous chemokine receptor Cxcr2 in zebrafish. Developmental & Comparative Immunology. 2017;67:57-65.
16. Sommer F, Torraca V, Meijer AH. Chemokine Receptors and Phagocyte Biology in Zebrafish. Frontiers in Immunology. 2020;11(325).
17. Hsu AY, Wang D, Gurol T, Zhou W, Zhu X, Lu H-Y, et al. Overexpression of microRNA-722 fine-tunes neutrophilic inflammation by inhibiting Rac2 in zebrafish. Disease models & mechanisms. 2017;10(11):1323-32.
18. Hsu AY, Wang D, Liu S, Lu J, Syahirah R, Bennin DA, et al. Phenotypical microRNA screen reveals a noncanonical role of CDK2 in regulating neutrophil migration. Proceedings of the National Academy of Sciences. 2019;116(37):18561.
19. Isles HM, Herman KD, Robertson AL, Loynes CA, Prince LR, Elks PM, et al. The CXCL12/CXCR4 Signaling Axis Retains Neutrophils at Inflammatory Sites in Zebrafish. Frontiers in Immunology. 2019;10(1784).
20. Zhou W, Cao L, Jeffries J, Zhu X, Staiger CJ, Deng Q. Neutrophil-specific knockout demonstrates a role for mitochondria in regulating neutrophil motility in zebrafish. Disease Models & Mechanisms. 2018;11(3):dmm033027.
21. Zhou W, Pal AS, Hsu AY-H, Gurol T, Zhu X, Wirbisky-Hershberger SE, et al. MicroRNA-223 Suppresses the Canonical NF-κB Pathway in Basal Keratinocytes to Dampen Neutrophilic Inflammation. Cell Reports. 2018;22(7):1810-23.
22. Conrad WH, Osman MM, Shanahan JK, Chu F, Takaki KK, Cameron J, et al. Mycobacterial ESX-1 secretion system mediates host cell lysis through bacterium contact-dependent gross membrane disruptions. Proceedings of the National Academy of Sciences of the United States of America. 2017;114(6):1371-6.
23. Li H, Yao G, Feng B, Lu X, Fan Y. Circ_0056618 and CXCR4 act as competing endogenous in gastric cancer by regulating miR-206. Journal of Cellular Biochemistry. 2018;119(11):9543-51.
24. Stahlhut C, Suárez Y, Lu J, Mishima Y, Giraldez AJ. miR-1 and miR-206 regulate angiogenesis by modulating VegfA expression in zebrafish. Development. 2012;139(23):4356.
25. Ulitsky I, Shkumatava A, Jan CH, Subtelny AO, Koppstein D, Bell GW, et al. Extensive alternative polyadenylation during zebrafish development. Genome Res. 2012;22(10):2054-66.

26. Zheng X, Ma YF, Zhang XR, Li Y, Zhao HH, Han SG. Circ_0056618 promoted cell proliferation, migration and angiogenesis through sponging with miR-206 and upregulating CXCR4 and VEGF-A in colorectal cancer. Eur Rev Med Pharmacol Sci. 2020;24(8):4190-202.
27. Döring Y, Pawig L, Weber C, Noels H. The CXCL12/CXCR4 chemokine ligand/receptor axis in cardiovascular disease. Frontiers in Physiology. 2014;5(212).
28. Walters KB, Green JM, Surfus JC, Yoo SK, Huttenlocher A. Live imaging of neutrophil motility in a zebrafish model of WHIM syndrome. Blood. 2010;116(15):2803-11.
29. Zou Y-R, Kottmann AH, Kuroda M, Taniuchi I, Littman DR. Function of the chemokine receptor CXCR4 in haematopoiesis and in cerebellar development. Nature. 1998;393(6685):595-9.
30. Oehlers SH, Cronan MR, Scott NR, Thomas MI, Okuda KS, Walton EM, et al. Interception of host angiogenic signalling limits mycobacterial growth. Nature. 2015;517(7536):612-5.
31. Yang C-T, Cambier CJ, Davis JM, Hall Christopher J, Crosier Philip S, Ramakrishnan L. Neutrophils Exert Protection in the Early Tuberculous Granuloma by Oxidative Killing of Mycobacteria Phagocytosed from Infected Macrophages. Cell Host & Microbe. 2012;12(3):301-12.
32. Papayannopoulos V. Neutrophil extracellular traps in immunity and disease. Nature Reviews Immunology. 2018;18(2):134-47.
33. García-Cuesta EM, Santiago CA, Vallejo-Díaz J, Juarranz Y, Rodríguez-Frade JM, Mellado M. The Role of the CXCL12/CXCR4/ACKR3 Axis in Autoimmune Diseases. Frontiers in Endocrinology. 2019;10(585).
34. Lopez MJ, Seyed-Razavi Y, Jamali A, Harris DL, Hamrah P. The Chemokine Receptor CXCR4 Mediates Recruitment of CD11c+ Conventional Dendritic Cells Into the Inflamed Murine Cornea. Investigative Ophthalmology & Visual Science. 2018;59(13):5671-81.
35. Tian X, Xie G, Xiao H, Ding F, Bao W, Zhang M. CXCR4 knockdown prevents inflammatory cytokine expression in macrophages by suppressing activation of MAPK and NF-κB signaling pathways. Cell & Bioscience. 2019;9(1):55.
36. Hoshino Y, Tse DB, Rochford G, Prabhakar S, Hoshino S, Chitkara N, et al. *Mycobacterium tuberculosis*-Induced CXCR4 and Chemokine Expression Leads to Preferential X4 HIV-1 Replication in Human Macrophages. The Journal of Immunology. 2004;172(10):6251-8.
37. Mendonça VA, Alvim de Melo GEB, Araújo MG, Borges VO, Costa RD, Martins-Filho OA, et al. Expression of the chemokine receptor CXCR4 on lymphocytes of leprosy patients. Brazilian Journal of Medical and Biological Research. 2011;44:1256-60.
38. Torraca V, Tulotta C, Snaar-Jagalska BE, Meijer AH. The chemokine receptor CXCR4 promotes granuloma formation by sustaining a mycobacteria-induced angiogenesis programme. Scientific reports. 2017;7:45061-.
39. Hajishengallis G, Wang M, Liang S, Triantafilou M, Triantafilou K. Pathogen induction of CXCR4/TLR2 cross-talk impairs host defense function. Proceedings of the National Academy of Sciences. 2008;105(36):13532-7.
40. Wang M, Ji Y, Cai S, Ding W. MiR-206 Suppresses the Progression of Coronary Artery Disease by Modulating Vascular Endothelial Growth Factor (VEGF) Expression. Med Sci Monit. 2016;22:5011-20.
41. Oehlers SH, Cronan MR, Beerman RW, Johnson MG, Huang J, Kontos CD, et al. Infection-Induced Vascular Permeability Aids Mycobacterial Growth. The Journal of Infectious Diseases. 2017;215(5):813-7.
42. Polena H, Boudou F, Tilleul S, Dubois-Colas N, Lecointe C, Rakotosamimanana N, et al. Mycobacterium tuberculosis exploits the formation of new blood vessels for its dissemination. Scientific Reports. 2016;6(1):33162.
43. Walton EM, Cronan MR, Cambier CJ, Rossi A, Marass M, Foglia MD, et al. Cyclopropane Modification of Trehalose Dimycolate Drives Granuloma Angiogenesis and Mycobacterial Growth through Vegf Signaling. Cell Host & Microbe. 2018;24(4):514-25.e6.

547 44. Arandjelovic S, Perry JSA, Lucas CD, Penberthy KK, Kim T-H, Zhou M, et al. A noncanonical role
548 for the engulfment gene ELMO1 in neutrophils that promotes inflammatory arthritis. Nature
549 Immunology. 2019;20(2):141-51.
550 45. Tamgue O, Gcanga L, Ozturk M, Whitehead L, Pillay S, Jacobs R, et al. Differential Targeting of
551 c-Maf, Bach-1, and Elmo-1 by microRNA-143 and microRNA-365 Promotes the Intracellular Growth of
552 Mycobacterium tuberculosis in Alternatively IL-4/IL-13 Activated Macrophages. Frontiers in
553 Immunology. 2019;10:421.
554 46. Taylor JL, Hattle JM, Dreitz SA, Troudt JM, Izzo LS, Basaraba RJ, et al. Role for Matrix
555 Metalloproteinase 9 in Granuloma Formation during Pulmonary *Mycobacterium tuberculosis*
556 Infection. Infection and Immunity. 2006;74(11):6135-44.
557 47. Liu Q, Zheng J, Yin D-D, Xiang J, He F, Wang Y-C, et al. Monocyte to macrophage differentiation-
558 associated (MMD) positively regulates ERK and Akt activation and TNF-α and NO production in
559 macrophages. Molecular Biology Reports. 2012;39(5):5643-50.
560 48. Hall C, Flores MV, Storm T, Crosier K, Crosier P. The zebrafish lysozyme C promoter drives
561 myeloid-specific expression in transgenic fish. BMC Developmental Biology. 2007;7(1):42.
562 49. Matty MA, Oehlers SH, Tobin DM. Live Imaging of Host–Pathogen Interactions in Zebrafish
563 Larvae. In: Kawakami K, Patton EE, Orger M, editors. Zebrafish: Methods and Protocols. New York, NY:
564 Springer New York; 2016. p. 207-23.
565 50. Duggin IG, Aylett CHS, Walsh JC, Michie KA, Wang Q, Turnbull L, et al. CetZ tubulin-like proteins
566 control archaeal cell shape. Nature. 2015;519(7543):362-5.
567 51. Iosifidis G, Duggin IG. Distinct Morphological Fates of Uropathogenic *Escherichia coli*
568 Intracellular Bacterial Communities: Dependency on Urine Composition and pH. Infection and
569 Immunity. 2020;88(9):e00884-19.
570 52. Wu RS, Lam II, Clay H, Duong DN, Deo RC, Coughlin SR. A Rapid Method for Directed Gene
571 Knockout for Screening in G0 Zebrafish. Developmental Cell. 2018;46(1):112-25.e4.

572

573 **Supporting information**

574 **S1 video. Neutrophil migration to infection in control embryos.**

575 **S2 video. Neutrophil migration to infection in miR-206 knockdown embryos.**

576 **S3 video. Neutrophil migration to sterile wound site in control embryos.**

577 **S4 video. Neutrophil migration to sterile wound site in miR-206 knockdown embryos.**